MADRID 2015
1-4 June 2015 | IFEMA Madrid

Th P5 12

Elastic Versus Viscoelastic Full Waveform Inversion of Near-offset and Wide-angle Data in the Presence of Attenuation

T. Belahi* (Institut de Physique du Globe de Paris (IPGP)), N. Fuji (Institut de Physique du Globe de Paris (IPGP)) & S.C. Singh (Institut de Physique du Globe de Paris (IPGP))

SUMMARY

Full Waveform Inversion (FWI) has proven to be a powerful tool to quantify the Earth's subsurface. In geological settings, such as gas clouds, gas sand, where attenuation is important, the application of FWI is still very challenging. We have developed a viscoelastic FWI in the time domain. In this paper, we investigate the need to properly account for attenuation when inverting long offset seismic data by comparing the results of elastic FWI applied to viscoelastic data and fully viscoelastic FWI. We carried experiments for short and long offset geometry of acquisition. The effect of attenuation could be divided into two parts: during wave propagation and during reflection. We find the presence of attenuation has a significant effect on wide-angle reflection data, both for reflection and propagation, but it has little or no effect on near-offset reflection data, suggesting that the elastic approximation is only sufficient when inverting pre-critical reflections and the attenuation should be taken into account while inverting wide-angle reflection data.

Introduction

Full waveform inversion (FWI) is recognised as a powerful tool to retrieve the quantitative structure of the subsurface. Due to the limitations of the physics embedded in FWI schemes, it is still challenging to image geologically interesting features such as gas clouds, hydrate bearing sediments, unconsolidated sediments or magma chambers, where anelastic effects are important. Attenuation can be included in FWI in the frequency domain by using complex velocities for acoustic media (e.g., Malinowski et al., 2011). Nevertheless, the implementation of attenuation in the elastic media and the time domain is not straightforward and has remained challenging. The time-domain FWI is interesting due to its implicit capability of extracting information on the full, frequency-wise, waveform data. Recently, there have been some synthetic studies of viscoelastic FWI for short offset (4 km) marine seismic data (e.g., Kurzmann et al., 2013, Barnes et al., 2014).

The success of FWI will depend on the availability of large offset seismic data, since they enable to invert both refracted and reflected waves (Shipp and Singh, 2002). In order to demonstrate the effect of attenuation, we calculate reflection coefficients as function of offset and attenuation (Fig. 1) (Bourbié et al.,1983). Figure 1 shows the amplitude of the reflection coefficients for an incident P and reflected P-waves for six different values of Qp above the reflector. The behaviour of the viscoelastic reflection coefficients is not impacted for incident angles smaller than the critical angle, whereas at larger angles, the dependence of Qp plays an important role, especially in the presence of low Qp values. This suggests that when inverting long offset datasets in the presence of high attenuation, there is a greater need to account for attenuation than for the inversion of short offset data. In other words, it seems feasible to extract information on attenuation structure when one inverts longer offset data. In this paper, we assess the importance of proper consideration of attenuation for FWI of long offset data.

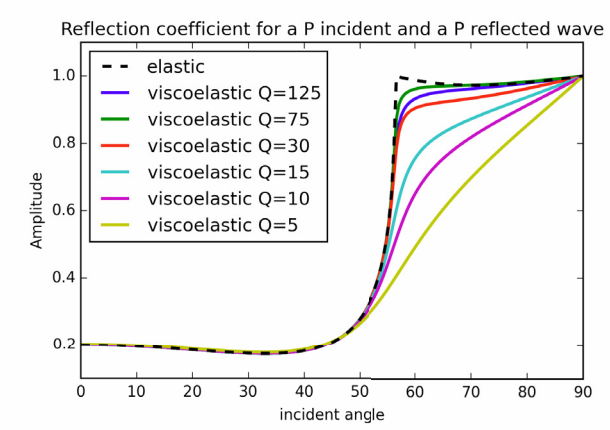

Figure 1 *Reflection coefficients as a function of incidence angle with varying values of Qp in the layer above the reflector. Other parameters are kept constant (Vp_1 =2500 m/s, Vs_1=1200 m/s, Qs_1=20, Vp_2=3000 m/s, Qp_2=50, Vs_2=1400 m/s, Qs_2=40 where 1 denotes the medium above and 2 the medium below the reflector). We can see that amplitudes of reflections at small incidence angles are not affected by Q variation whereas wider-angle data can suffer from low Q values.*

The attenuation can affect the seismic data in two ways: (1) during propagation of wave and (2) at reflection boundary. Here, we will mainly focus on the attenuation due to reflection effect.

Viscoelastic full waveform inversion in time domain

In order to model seismic wave propagation in a viscoelastic medium in the time domain, we have to incorporate a general formulation of the Hooke's law that accounts for the time dependence of stresses and strain in the propagation medium via time convolution such that:

$$\sigma^{ij}(\mathbf{x},t) = \int_{-\infty}^{+\infty} d\tau \Psi^{ijkl}(\mathbf{x},t-\tau)\dot{\varepsilon}^{kl}(\mathbf{x},t), \quad (1)$$

where σ_{ij} is stress, ε_{ij} is strain, Ψ^{ijkl} is the time-dependent stiffness tensor and the dot denotes time derivation.

We use Standard Linear Solids (SLS), constituted of a dashpot and springs to parameterise Ψ^{ijkl}. Superposing SLSs allows us to replace the convolution equations by a set of ordinary partial differential equations, including memory variables that account for the dissipation of energy over time

(Robertsson et al., 1994). In this study we use only one SLS to parameterise each cell of the model. This simplifies the mapping of the P- and S-wave velocities and the quality factors Qp and Qs to the Lamé parameters needed for the modelling.

The inversion consists in the minimisation of the misfit between the observed and synthetic data. We use the conjugate gradient technique introduced by Tarantola (1988) to minimise the misfit. The method iteratively updates the Vp, Vs, Qp and Qs parameters. We compute the gradient for 4 parameters: $\pi = \lambda + 2\mu$, μ at time 0^+ as well as $\Delta\pi$ and $\Delta\mu$, which account for the variation of π and μ over the propagation time. The resulting gradients are (for π):

$$\delta\pi(\mathbf{x}, 0^+) = -\int_{t_0}^{t_1} dt \overleftarrow{\varepsilon}_{ii} \overrightarrow{\varepsilon}_{jj}(\mathbf{x}, t) \quad \text{and} \quad \delta\Delta\pi(\mathbf{x}) = -\sum_{\ell=1}^{L^\pi} \int_{t_0}^{t_1} dt \overleftarrow{\varepsilon}_{ij} \overrightarrow{r}^{\ell}_{kl}(\mathbf{x}, t) \ , \tag{2}$$

where r_ℓ^{kl} are the memory variables that are governed by first order partial differential equations. Since Qp and Qs can be linked to the Lamé parameters using the relationship (Barnes et al., 2014):

$$Q_\nu = c + d\frac{\nu}{\Delta\nu}, \tag{3}$$

where *c* and *d* are two known constants that can be expressed in terms of the characteristic relaxation times of the model when using a single SLS, we can map the gradient on Lamé parameters to the set of parameters Vp, Vs, Qp and Qs:

$$\begin{pmatrix} \delta V_p \\ \delta V_s \\ \delta Q_p \\ \delta Q_s \end{pmatrix} = \begin{pmatrix} 2\rho V_p & 0 & \frac{2d\rho V_p}{Q_p - c} & 0 \\ 0 & 2\rho V_s & 0 & \frac{2d\rho V_s}{Q_s - c} \\ 0 & 0 & -\frac{dV_p^2\rho}{(Q_p - c)^2} & 0 \\ 0 & 0 & 0 & -\frac{dV_s^2\rho}{(Q_s - c)^2} \end{pmatrix} \begin{pmatrix} \delta\pi \\ \delta\mu \\ \delta\Delta\pi \\ \delta\Delta\mu \end{pmatrix} . \tag{4}$$

Synthetic experiment geometry

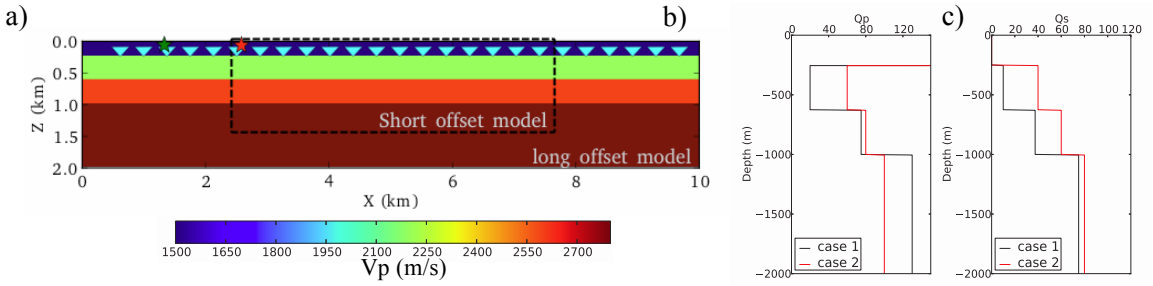

Figure 2 *a) The first geometry consists of 201 OBCs lying on the seafloor and spaced by 20 m covering 4km of offset and 20 shots spaced by 250 m at 20 m depth underwater. The second geometry consists of 451 OBCs also spaced by 20 m and 29 shots spaced every 250 m with a maximum source-receiver offset of 8 km. b) Qp profiles for the 2 scenarii. c) Qs profiles.*

In order to assess both the influence of attenuation and of the offsets contained in the data, we run four experiments with the same 2D velocity model with 3 flat layers under water (Fig. 2.a). We define two different profiles of attenuation (Fig.2.b and Fig.2.c): i) low values of Q and strong contrasts corresponding to a first layer of unconsolidated sediments lying on consolidated rocks; ii) high values for the Q and smaller contrasts of attenuation between layers. Both models are inverted with two different geometry of acquisition (Fig 2.a). Each dataset is inverted with a full elastic FWI scheme and a full viscoelastic scheme. We ran each experiment for 30 iterations.

Inversion results

For each experiment we invert the full gathers and the starting model for the attenuation parameters is a smooth version of the true model. Note that all inversions were performed for 2D models but only vertical profiles extracted at the centre of the model are displayed.

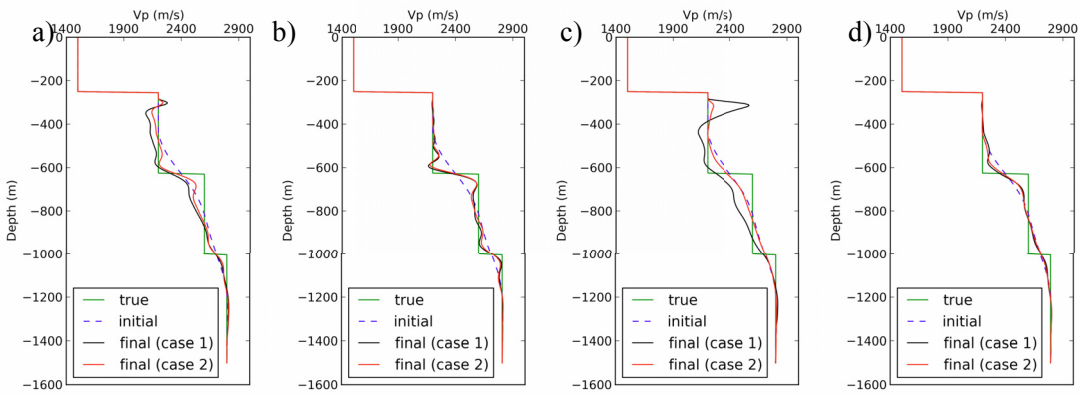

Figure 3 *Profiles of inverted P-wave velocities for a) elastic FWI of viscoelastic short offset data, b) viscoelastic FWI of viscoelastic data, c) elastic FWI of viscoelastic long offset data and d) viscoelastic FWI of viscoelastic data.*

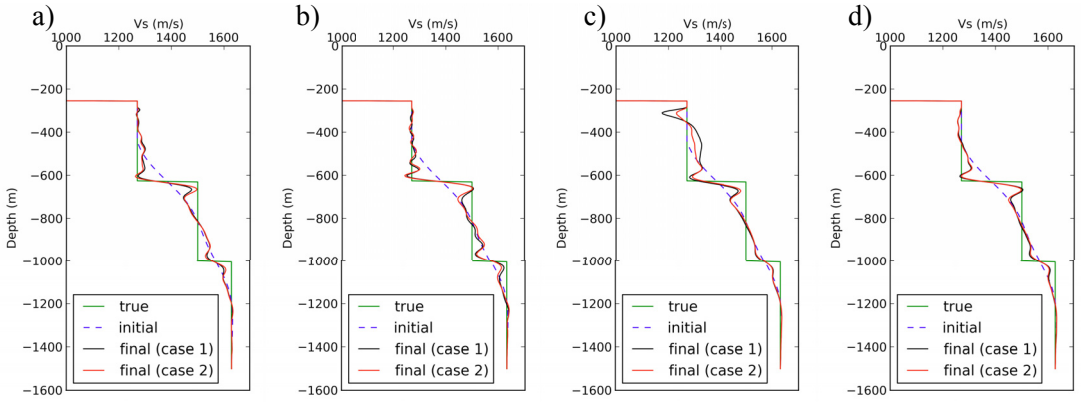

Figure 4 *Profiles of inverted S-wave velocities for a) elastic FWI of viscoelastic short offset data, b) viscoelastic FWI of viscoelastic data, c) elastic FWI of viscoelastic long offset data and d) viscoelastic FWI of viscoelastic data.*

Figures 3 and 4 show that the best inversion results are always obtained when attenuation is accounted for by the FWI scheme. However, the difference in the results is less dramatic when one inverts short offset data (Fig. 3.a and Fig. 3.b) than when one inverts long offset data (Fig 3.c and Fig.3.d). This indicates that the effect of attenuation at angles of incidence larger than the critical angle dominates the inversion. P-wave velocities display the strongest sensitivity to the attenuation, especially in the first layer; S-wave velocities are less impacted by not taking attenuation into account as shown by the comparison of Figure 3.c and Figure 4.c. We can also observe that for short offset data, the elastic inversion results are similar for the two different attenuation profiles (Fig 3.a and Fig.4.a). The elastic inversion results of long-offset data are hampered in the presence of higher attenuation values (Fig. 3.c and Fig 4.c). The worse case scenario is the elastic inversion of long offset data in the presence of strong attenuation.

Attenuation has two effects: the reflection effects and the transmission effect. Comparing Figures 5.c and 5.e, we observe at short offsets (up to 2 km) that the reflections are properly accounted for by the elastic scheme but not the primary arrival. Figures 5.d and 5.f show that at large offsets neither the primaries nor the reflections are properly matched by the elastic FWI scheme. Figure 1 shows that there is no reflection effect at short offsets, which explains that reflections are matched at short offsets by the elastic FWI scheme (Fig. 5.c). Figures 5.c and 5.d both have residuals coming from the improperly matched primaries because the transmission effect impacts both the short and long offsets. Reflections at long offsets are not properly matched by the elastic FWI scheme (Fig

5.d) because of the impact of attenuation on the reflection coefficient at wide angles of incidence shown in Figure 1.

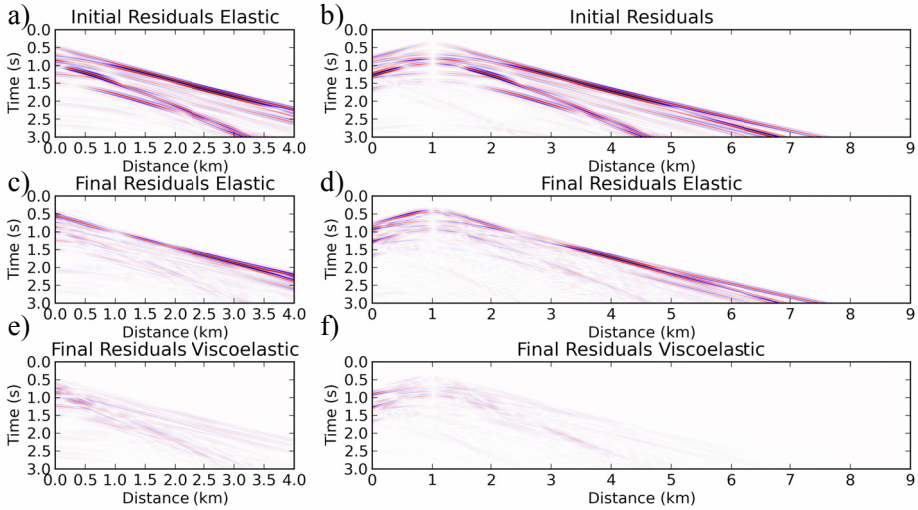

Figure 5 *Initial and final residuals obtained for the elastic inversion of viscoelastic data with short-offset geometry (a and c) and the long offset geometry (c and d). e) and f) are the final residuals for the viscoelastic inversion of viscoelastic data. For each experiment the attenuation profile corresponds to case 2. See Fig. 2. for the geometry of acquisition.*

Conclusions

We have developed and carried out viscoelastic waveform inversion in the time domain for 2D media. The synthetic case studies show that long offset data requires a proper treatment of anelasticity, regardless of its degree. While the elastic assumption can yield acceptable results to some extent when we invert short offset data in a less attenuating media, we should take into account attenuation when inverting short offset data in highly attenuating media. Furthermore, the impact of attenuation is less important on short offsets because it has no effect on reflections but is very important for long offset refractions especially just after the incident angle were attenuation impacts both reflected and transmitted waves. Not accounting for attenuation and applying elastic FWI to data that exhibits strong attenuation features may not converge to an acceptable model with the same acquisition geometry.

Acknowledgements

We thank the French National Research Agency (ANR) and the GPX industrial sponsors, CGG, Schlumberger and Total, for supporting this research.

References

Barnes, C., Charara, M., Williamson, P. [2014] P & S Wave Attenuation Effects on Full-Waveform Inversion for Marine Seismic Data, *SEG Annual Meeting*, Expanded Abstract

Bourbié, T., Gonzalez-Serrano, A. [1983] Synthetic seismograms in attenuating media. *Geophysics*, **48**(12)

Kurzmann, A., Przebindowska, A., Kohn, D., & Bohlen, T. [2013] Acoustic full waveform tomography in the presence of attenuation: a sensitivity analysis. *Geophysical Journal International*, **195**(2), p985–1000

Malinowski, M., Operto, S. and Ribodetti, A. [2011] High-resolution seismic attenuation imaging from wide-aperture onshore data by visco-acoustic frequency-domain full-waveform inversion. *Geophysical Journal International*, **186**(3)

Robertsson, J. O. a., Blanch, J. O. and Symes, W. W. [1994] Viscoelastic finite-difference modeling. *Geophysics*, **59**(9)

Shipp, R. M. and Singh, S. C. [2002] Two-dimensional full wavefield inversion of wide-aperture marine seismic streamer data, *Geophysical Journal International*, **151**, 325-344

Tarantola, A. [1988] Theoretical Background for the Inversion of Seismic Waveforms, Including Elasticity and Attenuation. *Pure and Applied geophysics*, **128**, p365-399